







**Correspondence of max-flow to the absolute permeability of porous systems**Ryan T. Armstrong ,\* Zakhar Lanetc , and Peyman Mostaghimi *School of Minerals and Energy Resources Engineering, University of New South Wales, Sydney,  
New South Wales 2052, Australia*Aleksandr Zhuravljov *Institute of Environmental and Agricultural Biology, University of Tyumen, Tyumen, Tyumen Oblast, Russia*Anna Herring  and Vanessa Robins *Research School of Physics, Australian National University, Canberra, Australian Capital Territory 2601,  
Australia*

(Received 27 July 2020; accepted 1 April 2021; published 14 May 2021)

The absolute permeability of porous media is an important parameter for various technological applications ranging from ground water hydrology to hydrocarbon recovery to microfluidics. There are scaling relationships between the geometric structure of a porous domain and its absolute permeability within a given class of structure. However, there exists no universal relationship between permeability and structure. We use network models of porous domains and apply the max-flow min-cut theorem to extract insights into the structures that most influence absolute permeability. The max-flow min-cut theorem states that the maximum flow through any network is exactly the sum of the edge weights that define the minimum cut. We hypothesize that the min-cut can be related to network permeability. We demonstrate that flow in porous media can be modeled as described by the max-flow min-cut theorem, which provides an approach to measure the absolute permeability of three-dimensional digital images of porous media. The max-flow of a network is found to correspond to its absolute permeability for over four orders of magnitude and identifies structural regions that result in significant energy dissipation. The findings are beneficial for the design of porous materials, as a subroutine for digital rock studies, the simplification of large network models, and further fundamental studies on the structure and flow properties of porous media.

DOI: [10.1103/PhysRevFluids.6.054003](https://doi.org/10.1103/PhysRevFluids.6.054003)**I. INTRODUCTION**

Absolute permeability is a fundamental parameter that quantifies the ease at which fluid flows through a porous domain [1,2]. It is a key design parameter for reservoir engineering, membrane systems, microfluidics, drug transport, packed bed reactors, soil systems, and various other porous medium applications [1,3–7]. The internal structure of porous materials is extremely diverse, ranging from isotropic to anisotropic domains, length scales ranging several orders of magnitude (submicrometer to meter), and topological structures with various degrees of connectivity [8–10]. Permeability is known to scale with porosity (or void fraction  $\phi$ ) for a given class of structure near a critical limit [11]. This scaling is widely applied via the Kozeny-Carman equation despite common errors observed for natural porous media [12–14]. These errors occur because porosity alone does not capture differences in pore size, surface area, and connectivity of the void space, which are

\*ryan.armstrong@unsw.edu.au

critical parameters controlling flow [15]. The structural complexity of porous media presents a significant challenge when trying to infer the absolute permeability of a porous system from porosity alone [16]. To reexamine the relationship between porous medium structures and permeability, we propose a graph theory approach [17] to study the max-flow min-cut of networks derived from three-dimensional x-ray microtomography (microcomputed tomography) images. While this work is aligned with previous pore-network modeling [18] and direct simulation [19] studies, the approach presented here provides an alternative perspective on the structural characteristics that control permeability, and thus a means to optimize and study porous structures, predict permeability from structure alone, and/or develop subroutines for optimization of numerical simulations.

It is well understood that the connectivity, porosity, surface area, and roughness of a porous structure strongly influence its absolute permeability and that one of these parameters alone is insufficient to characterize a medium [2]. One approach has been to modify the Kozeny-Carman equation via incorporation of fractal geometry characterization of the pore space [14,20]. Alternatively, percolation theory (in particular) has been used to study a wide variety of flow and transport problems [21]. For example, Katz and Thompson demonstrated that for geological materials permeability  $K$  is correlated to a critical pore radius  $r_c$ , which is the radius of the largest sphere that can percolate through the sample, defined as

$$K = cr_c^2 \frac{\sigma}{\sigma_0}, \quad (1)$$

where  $c$  is a constant,  $\sigma$  is the electrical conductivity of a brine-saturated sample, and  $\sigma_0$  is the electrical conductivity of the brine [22]. In Eq. (1),  $r_c$  captures the governing length scale and the formation factor  $\sigma/\sigma_0$  captures other morphological dependences. As shown by Scholz *et al.* for quasi-two-dimensional systems, the formation factor can be replaced by the genus per grain of the porous media to provide

$$K = cr_c^2 \left( \frac{1 - \chi_0}{N} \right)^\alpha, \quad (2)$$

where  $N$  is the number of grains,  $\chi_0$  is the Euler characteristic, and  $\alpha$  is a scaling parameter [23]. The Euler characteristic is a topological measure that describes the connectivity of an object [9]. In addition, other works have found correlations between porosity and permeability for a given class of structures and/or incorporated additional morphological features, such as the Minkowski functionals [16,24–26]. Although these formulations linking structural features of porous media to permeability are elegant, it has so far proven difficult to apply these formulations uniformly to materials of different classes and dimensionalities or to anisotropic materials given that the directionality of flow networks is not well captured by structural statistics.

We propose that flow in porous media can be generalized and modeled as described by the max-flow min-cut theorem, which relates the flow capacity through a weighted *directed* graph (max-flow) to a set of edges that disconnect it (min-cut); furthermore, the min-cut represents the subset of the porous medium network that dictates permeability. This will be demonstrated by testing a range of porous structures and demonstrating that energy loss is maximum across the min-cut. Likewise, we demonstrate that the max-flow corresponds to the absolute permeability of porous systems and that the min-cut provides structural characteristics that are key to understanding porous medium flow.

## II. THEORY

### A. Pore-network modeling

The absolute permeability  $K$  of a porous material is defined by Darcy's law as

$$K = \frac{\mu q L}{A(P_{\text{in}} - P_{\text{out}})}, \quad (3)$$

where  $\mu$  is the fluid viscosity,  $q$  is the total flow rate,  $L$  is the net distance from the inlet to the outlet,  $A$  is the cross-sectional area, and  $P$  is the pressure [1]. Equation (3) provides no way to relate

the porous structure to permeability because it is a continuum-scale formulation. In practice, flow experiments are commonly conducted to determine  $K$ , while the pore structure is treated as a black box [27], even though it is well known that permeability is highly dependent on the underlying porous structure [15]. Recent developments in pore-scale modeling and simulation, however, are providing further insights into the topological and geometrical structures that influence absolute permeability [28].

With pore-scale imaging, numerical simulation of flow within a given porous domain can be conducted to determine  $K$  [12]. With such an approach, the collective influence of pore geometry and topology on flow is captured. One method to solve for flow and pressure in a porous system is to decompose it into a network of pore throats and bodies [18,29] modeled by a graph with weighted nodes and edges. The absolute permeability of the rock calculated by using such a network is defined as  $K_{\text{PNM}}$  in the rest of the manuscript. In this graph, pore throats are edges and pore bodies are nodes and flow occurs through the edges. Therefore, the entire porous domain is defined by a graph  $G$  where the incidence matrix  $I(G)$  provides the connectivity relationship between edges and nodes; see Ref. [17] for formal definitions. This approach provides a unique opportunity to apply graph theory to better understand how absolute permeability is influenced by the porous structure of the media, as discussed in the next section. In the following text, we further explain how flow is modeled in  $G$ .

Hydrodynamic flow through  $G$  is calculated by considering the mass conservation principle, defined at each node  $i$  as

$$\sum_j q_{ij} = 0, \quad (4)$$

where  $q_{ij}$  is the flux through the edge connecting node  $i$  to node  $j$  and the sum is taken over all the edges incident to  $i$ . Flux can be defined by considering the conductivity  $C$  of edge  $e$  between connected nodes as

$$q_{ij} = \frac{C_{ij}}{\mu L_{ij}} (P_i - P_j), \quad (5)$$

where coupled indices  $ij$  are an alternative representation of a particular edge  $e$  ( $e = ij$ ). This notation requires that two pores are connected by only one throat. If there are multiple throats connecting two pores, these should be replaced by a single edge with effective conductivity and length values.

For laminar flow through a tube, conductivity is given analytically by the Hagen-Poiseuille equation defined as

$$C_{ij} = \frac{1}{8} \pi r_{ij}^4, \quad (6)$$

where  $r$  is the throat radius. The cylindrical shape of the throats is chosen for simulation instead of implementing shape factors to keep the model simple for this particular study. Based on Eq. (4), a linear system of equations describing the material balance around each node is defined as

$$P = \Delta_w^{-1} b, \quad (7)$$

where  $P$  is an array of unknown pressures at each node,  $\Delta_w$  is the discrete Laplacian matrix weighted by  $C_{ij}/\mu L_{ij}$ , and  $b$  is an array with  $F$  and  $-F$  at the inlet and outlet nodes, respectively, and zero for all other nodes. For graph  $G$ ,  $\Delta_w$  is found by

$$\Delta_w = IW I^T, \quad (8)$$

where  $W$  is a diagonal matrix of the hydraulic conductivity of each edge and  $I$  is the incidence matrix of  $G$ . The system of equations is solved for  $P$  at each node and then Eq. (3) is used to determine absolute permeability. Considering the number of arithmetic computations required to solve Eq. (7) by Gaussian elimination with  $N$  nodes, the complexity is  $O(N^3)$ . By using a sparse matrix approach, however, the complexity can be reduced to  $O(VN)$ , where  $V$  is the mean vertex degree.

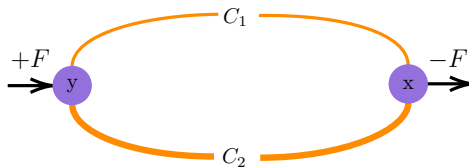


FIG. 1. Simple graph with flow  $F$  and local hydraulic conductivities  $C_1$  and  $C_2$  for the edges. Flow is distributed along the edges such that frictional energy loss is minimized.

### B. Max-flow min-cut

The max-flow min-cut theorem represents a duality between the maximum flow passing through a network from source to sink and the total capacity of a minimum cut for the network. A cut is any subset of edges whose removal disconnects the source from the sink and the total capacity is the sum of capacities (weights) of a subset of edges. The theorem has been applied to a variety of combinatorial optimization problems [30–33]. Finding max-flow corresponds to solving a linear problem, analogous to the linear system of equations used to solve flow through a network model [33,34]. The simplest abstraction of a porous medium is the decomposition of its structure into a discrete set of edges and nodes [35] where flow is along the edges between the nodes. Flow  $f_e$  through each edge is controlled by local hydraulic conductivity  $C_e$  and the total flow  $F$  through the network is governed by an upscaled effective hydraulic conductivity of the entire network. For the simple network displayed in Fig. 1, the mechanical energy balance between enthalpy and frictional energy from node  $y$  to  $x$  is

$$E = \frac{\Delta P}{\rho} = \sum_e X_e f_e^2 = \sum_e E_e, \quad (9)$$

where  $\rho$  is the fluid density,  $\Delta P$  is the pressure drop between two nodes,  $X_e$  is an empirical friction factor for edge  $e$ , and  $E_e$  is the energy loss for a particular edge  $e$ . The total flow is also governed by  $F \propto C_T \Delta P$ , where  $C_T$  is the upscaled effective hydraulic conductivity. The local flows  $f_e$  are distributed along the edges such that  $E$  for the entire system is minimized. The flow is easily shown to be unique by solving a linear system of equations using the conservation of mass principle. The edges that take the largest  $f_e$  while maintaining a minimum  $E$  are the edges contributing significantly to energy dissipation. These edges are key structural features of the network that contribute to absolute permeability.

For instance, a simple graph depicted in Fig. 2 consists of eight edges and seven nodes. Each edge is characterized by a maximum flow capacity represented by the edge width and additionally annotated by the capacity magnitude. The external nodes labeled as  $y$  and  $x$  are the source and sink, correspondingly. Considering this particular graph, the total max-flow capacity of the min-cut subset is 3, which is equal to the total max-flow capacity of the whole graph. Various search algorithms can be used to find the min-cut subset, as discussed in the next paragraph.

For graph  $G$ , edge weights are defined by Eq. (6). We hypothesize that the total weight of the edges  $C_t$  from the min-cut corresponds to the effective hydraulic conductivity of the network. To find the min-cut of  $G$ , we use the Edmonds-Karp algorithm from the NetworkX PYTHON package [36]. The resulting max-flow capacity  $C_t$  is treated as the network permeability by

$$K_{\text{Edm}} = \frac{C_t}{A}, \quad (10)$$

where  $A$  is the samples cross-sectional area. A derivation of Eq. (10) is provided in the Appendix. The Edmonds-Karp algorithm is a modified version of the standard Ford-Fulkerson algorithm and has a runtime complexity of  $O(M^2N)$ , where  $M$  is the total number of edges. However, more

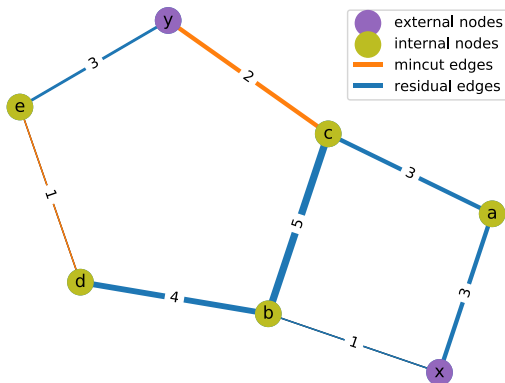


FIG. 2. Simple two-dimensional example that illustrates how the max-flow min-cut theorem can be employed.

advanced algorithms that approximate max-flow on undirected graphs can achieve complexity of  $O(N^{3/2})$  with the fastest known algorithm breaking the  $O(N^{3/2})$  complexity barrier [33].

Overall, the source code for the presented workflow is available via the GitHub repository in [37].

### III. POROUS MEDIA

We used porous medium images from the Network Generation Comparison Forum [38] provided by the National Laboratory for X-ray Micro Computed Tomography (CTLab) at the Australian National University. The images consist of a silica sphere pack, Castlegate sandstone, an unconsolidated sand pack, and Mt. Gambier limestone. Each data set is a cubic segmented image of  $512^3$  voxels. The silica sphere pack ( $\phi = 0.38$ ) consists of 1.59-mm-diameter beads imaged at  $17.5 \mu\text{m}$  resolution. The Castlegate sample ( $\phi = 0.21$ ) is an outcrop sandstone from southeastern Utah, USA that was imaged at  $5.6 \mu\text{m}$  resolution. The sand pack ( $\phi = 0.36$ ) is a poorly sorted unconsolidated fluvial sand from southern Australia imaged at  $9.2 \mu\text{m}$  resolution. Mt. Gambier limestone ( $\phi = 0.42$ ) is a fossiliferous outcrop carbonate imaged at  $3.0 \mu\text{m}$  resolution. All of the porous systems are displayed in Fig. 3.

In addition to the imaged porous systems, a selection of artificial porous systems were generated to provide a broader range of permeability values. The artificial media were generated using a method implemented in the PYTHON package PoreSpy [39]. The method generates an image by randomly placing amorphous blobs within a three-dimensional domain to a specified porosity. The generated images were  $512^3$  voxels in size. Figure 4 presents the range of porous systems that was generated.

### IV. RESULTS AND DISCUSSION

The pore network extracted for the Castlegate sandstone is displayed in Fig. 5 along with the edges and min-cut in Fig. 6. The pressures within each node and edge are also displayed in both figures. The pressure gradient is observed to be slightly nonuniform across the sample where the gradient is stronger along the bottom right of the sample than the top right. This difference can be observed as a slight diagonal plane indicated by a transition from high pressure (dark red) to intermediate pressures (pink). This plane also corresponds to the throats (edges) that were identified as the min-cut, as can be observed in Fig. 6.

The distributions of edge (throat) radii for the min-cut subsets are compared to the critical radius  $r_c$  for each real rock sample (see Fig. 7). The critical radius is calculated from the digital image

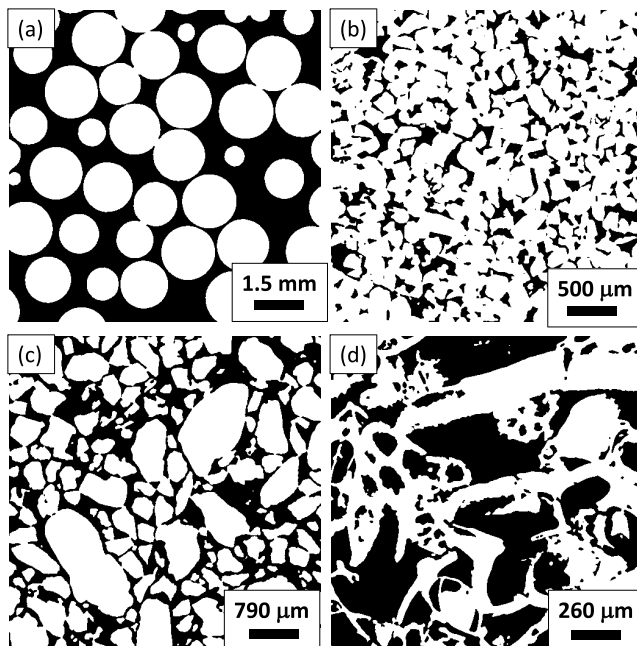


FIG. 3. Porous media utilized for the study: (a) silica sphere pack, (b) Castlegate sandstone, (c) unconsolidated sand pack, and (d) Gambier limestone. The displayed images are  $512 \times 512$  pixels and black represents void space.

as the largest sphere that can percolate through the pore space [40], which corresponds to  $r_c$  from Eq. (1). The edge radii along the min-cut are generally less than  $r_c$ , with  $r_c$  typically matching the maximum values of edge radii within the min-cut. The histograms also demonstrate that a large number of smaller edges contribute to the max-flow, while only a significantly smaller number of larger edge radii also contribute. These larger edge radii correspond to  $r_c$ ; however, the smaller edges also contribute to the max-flow and are likely to make an important contribution to absolute permeability, as will be discussed when considering energy loss within the min-cut.

In Fig. 8 we compare the absolute permeabilities determined by max-flow [Eq. (10)] to those determined by pore-network modeling [Eq. (3)]. For a range of permeabilities spanning five orders of magnitude, there is agreement between  $K_{Edm}$  and  $K_{PNM}$  with an average error of around 25%. These results suggest that the total weight of the edges in the min-cut corresponds to the absolute permeability and that in most cases, max-flow provides permeability values that are slightly less than that provided by solving the pore-network model. Permeability values for the real rock samples are provided in Table I, showing that  $K_{Edm}$  underpredicts permeability within a range of relative errors

TABLE I. Permeability of real samples obtained using pore-network modeling and the max-flow min-cut theorem.

Sample	$K_{PNM}$ (darcy)	$K_{Edm}$ (darcy)	Relative error
silica sphere pack	419.41	355.54	0.15
Castlegate sandstone	0.23	0.19	0.18
unconsolidated sand pack	10.68	10.13	0.10
Gambier limestone	3.62	1.49	0.59

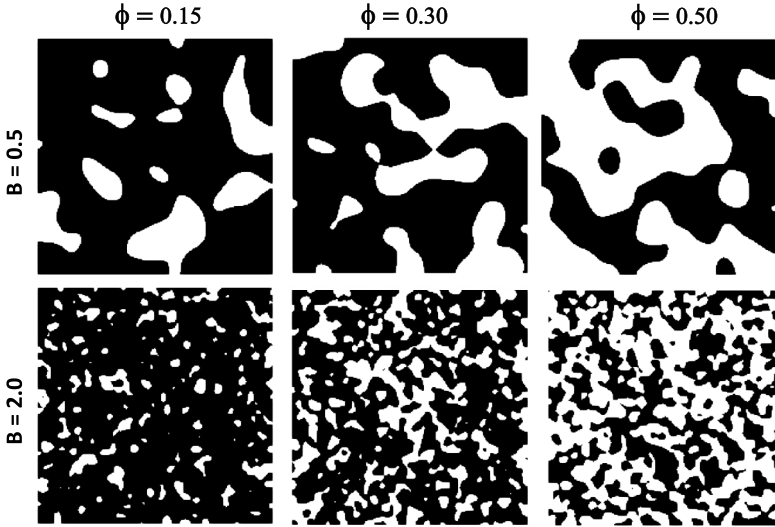


FIG. 4. Two-dimensional slices of artificial three-dimensional porous samples generated using PoreSpy where  $B$  is blobbiness and  $\phi$  is porosity. The displayed images are  $512 \times 512$  pixels and black represents void space. The image resolution is  $1 \mu\text{m}$  per pixel.

from 0.15 to 0.59. Relative error is measured as  $(K_{\text{PNM}} - K_{\text{Edm}})/K_{\text{PNM}}$ . Overall, the trend between  $K_{\text{Edm}}$  and  $K_{\text{PNM}}$  is consistent for the tested real rock samples and artificial porous domains.

The min-cut is a contraction of the edges to a single subset. This means that the min-cut spans from the inlet node at  $P_{\text{in}}$  to the outlet node at  $P_{\text{out}}$ , analogous to a bundle of capillary tubes or throats in parallel. For example, in Fig. 2, the min-cut subset includes edges 2 and 1 and all other edges are contracted, which would result in a min-cut network similar to that presented in Fig. 1. The max-flow  $C_t$  of the min-cut subset is 3. The implication is that an effective conductivity of  $C_t$  is applied over the entire network, which results in a constant pressure gradient. Depending on the specific geometrical parameters of the network, this assumption results in differences between  $K_{\text{PNM}}$  and  $K_{\text{Edm}}$ . For networks with relatively straight flow paths but a large variation in edge conductivities

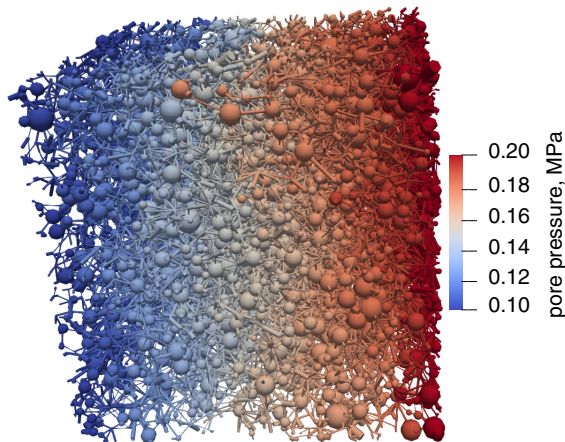


FIG. 5. Pore network extracted from the image of Castlegate sandstone.

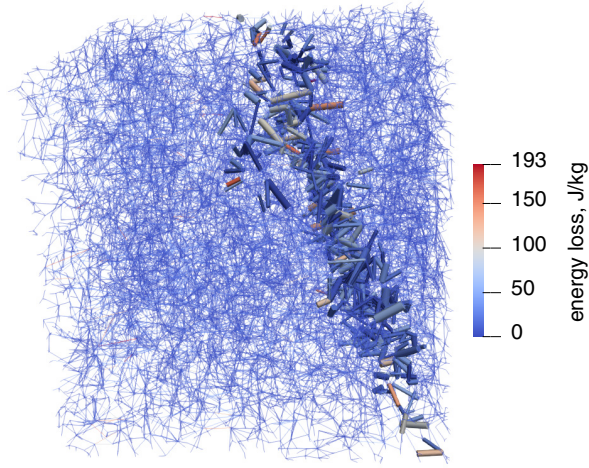


FIG. 6. Throat (edge) energy loss of Castlegate sandstone. Pore nodes are hidden while min-cut throats are highlighted.

along the flow path, a constant pressure gradient along the sample is not expected. As demonstrated in the Appendix, this type of network results in  $K_{\text{PNM}} > K_{\text{Edm}}$ . For networks with highly tortuous paths, where the total flow length is greater than the macroscopic sample length  $L$ , the contrary is expected, as demonstrated in the Appendix, i.e.,  $K_{\text{PNM}} < K_{\text{Edm}}$ . As observed in Fig. 8, the dominant

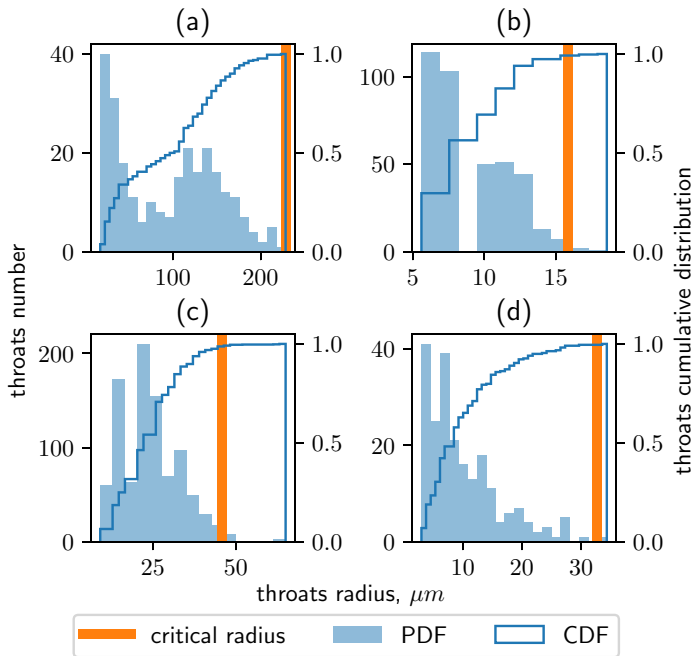


FIG. 7. Comparison of min-cut throat (edge) radii distribution of real porous media with their critical pore radii: (a) silica sphere pack with  $r_c = 228.5 \mu\text{m}$ , (b) Castlegate sandstone with  $r_c = 15.8 \mu\text{m}$ , (c) unconsolidated sand pack with  $r_c = 45.9 \mu\text{m}$ , and (d) Gambier limestone with  $r_c = 32.7 \mu\text{m}$ .



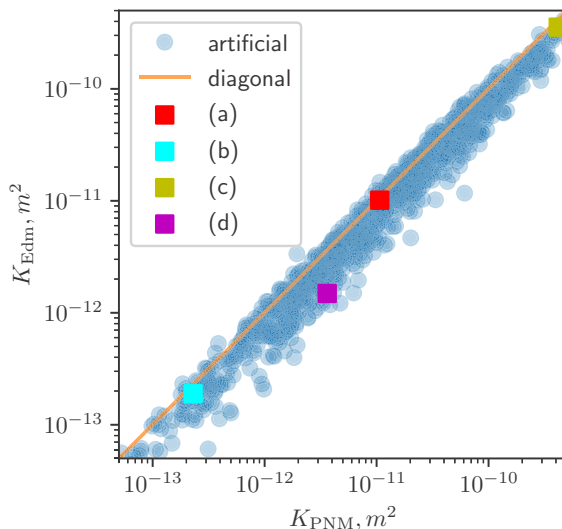


FIG. 8. Comparison between absolute permeability determined by max-flow min-cut theory  $K_{\text{Edm}}$  and solving the pore-network model  $K_{\text{PNM}}$ : (a) silica sphere pack, (b) Castlegate sandstone, (c) unconsolidated sand pack, and (d) Gambier limestone.

outcome is that  $K_{\text{PNM}} \gtrsim K_{\text{Edm}}$ , which suggests that the variation in edge conductivities along the flow path is the main geometrical feature of the network that results in the observed discrepancy.

The energy loss over the entire sample and that occurring in the min-cut can be compared to observe where the most energy dissipation occurs. We evaluate the average energy loss per throat  $E_{\text{av}}$  and per throat length  $E_{\text{av}}^L$  as

$$E_{\text{av}} = \frac{\sum_e^M E_e L_e}{\sum_e^M L_e}, \quad (11)$$

$$E_{\text{av}}^L = \frac{M E_{\text{av}}}{\sum_e^M L_e}, \quad (12)$$

where  $M$  is the number of edges that can correspond to the entire sample or a min-cut subset. The values are reported in Table II, where both averaging methods demonstrate that significantly more energy dissipation occurs across the min-cut than that observed on average in the sample. The reported deviation value is the relative difference between the min-cut and the entire domain. As shown in Eq. (9), the energy dissipation corresponds to a pressure drop resulting in a 2.51–16.3 times pressure drop across the min-cut compared to that observed on average in the entire sample.

TABLE II. Average energy loss per throat and per throat length for the min-cut and the entire sample.

Sample	$E_{\text{av}}$ ( $10^2$ J/kg)			$E_{\text{av}}^L$ ( $10^6$ J/(kg m))		
	Entire	Cut	Deviation	Entire	Cut	Deviation
silica sphere pack	10.57	29.77	2.82	1.07	2.52	2.36
Castlegate sandstone	0.08	0.49	6.23	0.05	0.25	5.12
unconsolidated sand pack	0.48	1.21	2.51	0.17	0.35	2.11
Gambier limestone	0.55	8.89	16.3	0.48	5.45	11.46

This is also qualitatively observed in Figs. 5 and 6, where it can be observed that a significant pressure drop occurs over the min-cut subset.

When comparing Tables I and II there is an observable trend between relative error and the deviation between energy dissipation across the entire sample and that across the min-cut subset. Take, for example, Gambier limestone, which has the highest relative error of 0.59 and highest deviation of 11.46. This links back to the min-cut being a contraction of the edges to a single subset. For fluid flow the conductivity and the distance from inlet to outlet determines the pressure drop. When a highly dissipative min-cut is identified, this conductivity is applied over the entire sample length to determine the pressure drop and subsequent permeability. However, there are fewer dissipative regions in the sample, and thus the actual pressure drop over the sample would be smaller. Therefore,  $K_{\text{PNM}} > K_{\text{Edm}}$  is a common outcome, as observed in Fig. 8 and explained further in the Appendix.

## V. CONCLUSION

By using the max-flow min-cut theorem, we have demonstrated that an entire pore network can be represented by a subset of parallel edges (min-cut) that is roughly 50 times less than the entire number of edges in the network. We are able to make the following key observations relevant to the min-cut of edges.

(i) Energy dissipation is significantly more along the min-cut than that observed on average throughout an entire porous structure.

(ii) The min-cut domain consists of edge radii less than or equal to the critical radius obtained from percolation theory.

(iii) The max-flow corresponds to absolute permeability for over four orders of magnitude.

(iv) The min-cut can be treated as parallel edges, unlike a pore network, where the edges are connected in an arbitrary way.

(v) The relative difference between permeability estimated by Eq. (10) and the value obtained from Eq. (3) can be explained by the variation in edge conductivities and the tortuosity of the flow path.

Future work should focus on the issue of how the pore-network simplification process impacts both the Laplacian solution for  $P$  and the min-cut max-flow determination. The network model in the presented work is the same for both computations, so it does not introduce any issues here. However, network generation is likely to introduce discrepancies when results of physical experiments and/or direct numerical simulations are compared to the min-cut max-flow of a network model, as observed in previous works on pore-network models that compare simulation results to physical measurements [41,42]. To address this issue, further work is required to determine topological parameters that are stable during network simplification to provide reliable insights into the physical relation between effective properties and pore-space topology. In our opinion, persistent homology would be a fruitful path forward in this respect [40,43,44].

The computational time for the min-cut solution is more demanding than solving the linear system of equations using a sparse matrix. The solution, however, provides a richer set of details on structural characteristics that impact absolute permeability, and thus porous medium flows. The max-flow min-cut algorithm could be used as a subroutine for numerical methods applied to porous media images. There are many ways to account for hydraulic conductance through various shape factors. To tune direct flow simulations, it can be enough to first vary hydraulic conductance using only the min-cut subset, which is a fast and simple procedure. This would be especially beneficial for large pore networks, greater than  $1000^3$  nodes. In addition, the identification of structural domains that cause significant energy dissipation provides a means to design and optimize porous systems for various applications, such as filtration, microfluidics, and/or packed bed reactors. For direct simulations of flow on microcomputed tomography images, regions of high dissipation could also highlight regions with numerical error and/or resolution issues that need to be identified to improve simulation and/or image segmentation quality. Tight constrictions in porous medium

images that are not fully resolved but contribute significantly to absolute permeability could result in simulation error. Segmentation quality and grid refinement within the min-cut domain would be important considerations for accurate numerical simulations and could be performed efficiently in an iterative way before applying to the entire domain. Finally, the max-flow min-cut theorem provides a way to characterize flow at a given length scale, providing a means to simplify a porous network into a basic subset that impacts flow. These findings demonstrate how the max-flow min-cut theorem can be used to study porous medium flows providing an alternative perspective on the structural characteristics that impact absolute permeability and applied approaches for digital rock studies.

### ACKNOWLEDGMENTS

V.R. gratefully acknowledges funding from Australian Research Council Grant No. FT140100604. A.H. acknowledges Australian Research Council Grant No. DE180100082 and the ANU/UNSW Digicore Research Consortium.

### APPENDIX: RELATING $K_{\text{PNM}}$ AND $K_{\text{Edm}}$

We start with Eq. (3). As before,  $L$  and  $A$  are the length and cross-sectional area of the core sample,  $q$  is the overall flow rate which is held constant at the inlet and outlet with values of  $F$  and  $-F$ , respectively, and  $P_{\text{in}} - P_{\text{out}}$  is the resulting pressure drop across the sample. For a network model, this pressure difference is found by solving the system of linear equations (7), which reflects the connectivity of the network and involves the edge weights  $C_{ij}/\mu L_{ij}$  as parameters. We will use  $K_{\text{PNM}}$  to refer to the permeability computed with this method.

Our minimum-cut approximation for permeability  $K_{\text{Edm}} = C_t/A$  is derived as follows. We know that the flux through the minimum cut edges can be added in parallel (no edges are connected in series) and that the total flux through the min-cut is the same as the value  $F$  maintained at the inlet and outlet. Using (5), we see that

$$\begin{aligned} K &= \frac{\mu L}{A} \frac{1}{P_{\text{in}} - P_{\text{out}}} \sum_{\text{cut}} C_{ij} \frac{P_i - P_j}{\mu L_{ij}} \\ &= \frac{1}{A} \sum_{\text{cut}} \left[ C_{ij} \frac{L}{P_{\text{in}} - P_{\text{out}}} \frac{P_i - P_j}{L_{ij}} \right]. \end{aligned}$$

If we now assume that the ratio  $L/\Delta P$  is constant across the whole sample, we see that

$$K \simeq \frac{1}{A} \sum_{\text{cut}} C_{ij} = K_{\text{Edm}}. \quad (\text{A1})$$

In the calculations of  $K_{\text{PNM}}$  and  $K_{\text{Edm}}$  summarized in Fig. 8, we see that this approximation is surprisingly good and that for most *but not all* samples  $K_{\text{PNM}} > K_{\text{Edm}}$ .

To understand the geometric parameters influencing the difference between  $K_{\text{PNM}}$  and  $K_{\text{Edm}}$  we consider the simple model of two pipes in series. As a network model, we have three nodes  $v_{\text{in}}$ ,  $v$ , and  $v_{\text{out}}$  and two edges  $e_1$ , joining  $v_{\text{in}}$  to  $v$ , and  $e_2$ , joining  $v$  to  $v_{\text{out}}$ . The conductivities associated with these edges are given by  $C_1 > C_2$  and lengths are  $L_1$  and  $L_2$ . We will allow the possibility that the sample length  $L < L_1 + L_2$ .

Solving the system of equations defined by  $\Delta_w P = b$ , we find the pressure at  $v$  is a free parameter and that

$$\begin{aligned} P_{\text{in}} &= F \frac{\mu L_1}{C_1} + P_v, \\ P_{\text{out}} &= -F \frac{\mu L_2}{C_2} + P_v, \text{ so } P_{\text{in}} - P_{\text{out}} = \mu F \left[ \frac{L_1}{C_1} + \frac{L_2}{C_2} \right]. \end{aligned}$$

Using this pressure drop in the expression for permeability, we obtain

$$\begin{aligned} K_{\text{PNM}} &= \frac{L}{A} \frac{C_1 C_2}{L_1 C_2 + L_2 C_1} \\ &= \frac{C_2}{A} \frac{L}{L_2 + L_1 \frac{C_2}{C_1}}. \end{aligned}$$

Since we choose  $C_1 > C_2$ , the first term in the above expression is  $K_{\text{Edm}}$  and the second term determines how well  $K_{\text{Edm}}$  approximates  $K_{\text{PNM}}$ .

We can make two limiting case studies of the relative values for  $L_1$ ,  $L_2$ ,  $L$ ,  $C_1$ , and  $C_2$ .

(i) Suppose the pipes are straight and the same length so that  $L_1 = L_2 = l$  and  $L = 2l$ . Then

$$K_{\text{PNM}} = K_{\text{Edm}} \frac{2}{1 + \frac{C_2}{C_1}},$$

and we see that if  $C_1 = C_2$ , then  $K_{\text{PNM}} = K_{\text{Edm}}$ , while in the limit  $C_1 \gg C_2$ ,  $K_{\text{PNM}} \rightarrow 2K_{\text{Edm}}$ .

(ii) Now suppose  $C_1 = C_2$ , but the pipes are not straight so  $(L_1 + L_2)/L = \tau > 1$  with  $\tau$  being a tortuosity parameter. Then

$$K_{\text{PNM}} = K_{\text{Edm}} \frac{L}{L_1 + L_2} = \frac{K_{\text{Edm}}}{\tau}.$$

The first case above suggests that for porous medium samples with fairly straight flow paths, but a large variation in the conductivities along a flow path, we expect  $K_{\text{PNM}} > K_{\text{Edm}}$ . The second case shows that for  $K_{\text{PNM}} < K_{\text{Edm}}$ , the sample should have highly tortuous flow paths with their total length much greater than the macroscopic sample length  $L$ .

- 
- [1] J. Bear and Y. Bachmat, *Introduction to Modeling of Transport Phenomena in Porous Media*, Theory and Applications of Transport in Porous Media Vol. 4 (Springer Science and Business Media, New York, 2012).
- [2] D. Tiab and E. C. Donaldson, *Petrophysics: Theory and Practice of Measuring Reservoir Rock and Fluid Transport Properties* (Gulf Professional Publishing, Oxford, 2015).
- [3] X. Yang, A. Fane, and K. Soldenhoff, Comparison of liquid membrane processes for metal separations: Permeability, stability, and selectivity, *Ind. Eng. Chem. Res.* **42**, 392 (2003).
- [4] E. J. Anderson, S. M. Kreuzer, O. Small, and M. L. K. Tate, Pairing computational and scaled physical models to determine permeability as a measure of cellular communication in micro- and nano-scale pericellular spaces, *Microfluid. Nanofluid.* **4**, 193 (2008).
- [5] M. A. Knackstedt, C. H. Arns, T. J. Senden, and K. Gross, Structure and properties of clinical coralline implants measured via 3D imaging and analysis, *Biomaterials* **27**, 2776 (2006).
- [6] E. Rabot, M. Wiesmeier, S. Schlüter, and H.-J. Vogel, Soil structure as an indicator of soil functions: A review, *Geoderma* **314**, 122 (2018).
- [7] A. Gerami, Y. Alzahid, P. Mostaghimi, N. Kashaninejad, F. Kazemifar, T. Amirian, N. Mosavat, M. E. Warkiani, and R. T. Armstrong, Microfluidics for porous systems: Fabrication, microscopy and applications, *Transp. Porous Media* **130**, 277 (2019).
- [8] K. Nordahl and P. S. Ringrose, Identifying the representative elementary volume for permeability in heterolithic deposits using numerical rock models, *Math. Geosci.* **40**, 753 (2008).
- [9] R. T. Armstrong, J. E. McClure, V. Robins, Z. Liu, C. H. Arns, S. Schlüter, and S. Berg, Porous media characterization using Minkowski functionals: Theories, applications and future directions, *Transp. Porous Media* **130**, 305 (2019).
- [10] K. Wu, M. I. Van Dijke, G. D. Couples, Z. Jiang, J. Ma, K. S. Sorbie, J. Crawford, I. Young, and X. Zhang, 3D stochastic modelling of heterogeneous porous media—Applications to reservoir rocks, *Transp. Porous Media* **65**, 443 (2006).

- [11] R. Hilfer, Local-porosity theory for flow in porous media, *Phys. Rev. B* **45**, 7115 (1992).
- [12] P. Mostaghimi, M. J. Blunt, and B. Bijeljic, Computations of absolute permeability on micro-CT images, *Math. Geosci.* **45**, 103 (2013).
- [13] J. Bear, *Dynamics of Fluids in Porous Media* (Courier, Chelmsford, 2013).
- [14] P. Xu and B. Yu, Developing a new form of permeability and Kozeny-Carman constant for homogeneous porous media by means of fractal geometry, *Adv. Water Resour.* **31**, 74 (2008).
- [15] C. F. Berg, Permeability description by characteristic length, tortuosity, constriction and porosity, *Transp. Porous Media* **103**, 381 (2014).
- [16] P. A. Slotte, C. F. Berg, and H. H. Khanamiri, Predicting resistivity and permeability of porous media using Minkowski functionals, *Transp. Porous Media* **131**, 705 (2020).
- [17] B. Bollobás, *Modern Graph Theory*, Graduate Texts in Mathematics Vol. 184 (Springer Science and Business Media, New York, 2013).
- [18] M. J. Blunt, Flow in porous media—Pore-network models and multiphase flow, *Curr. Opin. Colloid Interface Sci.* **6**, 197 (2001).
- [19] P. Meakin and A. M. Tartakovsky, Modeling and simulation of pore-scale multiphase fluid flow and reactive transport in fractured and porous media, *Rev. Geophys.* **47**, 1 (2009).
- [20] H. Pape, C. Clauser, and J. Iffland, Permeability prediction based on fractal pore-space geometry, *Geophysics* **64**, 1447 (1999).
- [21] M. Sahimi, *Applications of Percolation Theory* (CRC, Boca Raton, 1994).
- [22] A. J. Katz and A. H. Thompson, Quantitative prediction of permeability in porous rock, *Phys. Rev. B* **34**, 8179(R) (1986).
- [23] C. Scholz, F. Wirner, J. Götz, U. Råde, G. E. Schröder-Turk, K. Mecke, and C. Bechinger, Permeability of Porous Materials Determined from the Euler Characteristic, *Phys. Rev. Lett.* **109**, 264504 (2012).
- [24] Z. Liu, J. E. McClure, and R. T. Armstrong, Influence of wettability on phase connectivity and electrical resistivity, *Phys. Rev. E* **98**, 043102 (2018).
- [25] R. Hilfer, Review on scale dependent characterization of the microstructure of porous media, *Transp. Porous Media* **46**, 373 (2002).
- [26] C. Scholz, F. Wirner, M. A. Klatt, D. Hirneise, G. E. Schröder-Turk, K. Mecke, and C. Bechinger, Direct relations between morphology and transport in Boolean models, *Phys. Rev. E* **92**, 043023 (2015).
- [27] C. McPhee, J. Reed, and I. Zubizarreta, *Core Analysis: A Best Practice Guide* (Elsevier, Amsterdam, 2015).
- [28] M. J. Blunt, B. Bijeljic, H. Dong, O. Gharbi, S. Iglauer, P. Mostaghimi, A. Paluszny, and C. Pentland, Pore-scale imaging and modelling, *Adv. Water Resour.* **51**, 197 (2013).
- [29] S. Bakke and P.-E. Øren, 3-D pore-scale modelling of sandstones and flow simulations in the pore networks, *SPE J.* **2**, 136 (1997).
- [30] Y. Boykov and V. Kolmogorov, An experimental comparison of min-cut/max-flow algorithms for energy minimization in vision, *IEEE Trans. Pattern Anal.* **26**, 1124 (2004).
- [31] T. Leighton and S. Rao, Multicommodity max-flow min-cut theorems and their use in designing approximation algorithms, *J. ACM* **46**, 787 (1999).
- [32] L. R. Ford Jr., and D. R. Fulkerson, Maximal flow through a network, *Canadian J. Mathematics* **8**, 399 (1956).
- [33] P. Christiano, J. A. Kelner, A. Madry, D. A. Spielman, and S.-H. Teng, *Proceedings of the Forty-Third Annual ACM Symposium on Theory of Computing, San Jose, 2011* (ACM, New York, 2011), pp. 273–282.
- [34] I. Fatt, The network model of porous media, *Trans. AIME* **207**, 144 (1956).
- [35] J. H. van der Linden, G. A. Narsilio, and A. Tordesillas, Machine learning framework for analysis of transport through complex networks in porous, granular media: A focus on permeability, *Phys. Rev. E* **94**, 022904 (2016).
- [36] A. Hagberg, P. Swart, and D. S. Chult, Exploring network structure, dynamics, and function using NetworkX, Los Alamos National Laboratory Report No. LA-UR-08-05495, 2008 (unpublished).
- [37] [AleksZhuravlyov/mincut\\_maxflow\\_pnm](https://www.digitalrockportal.org/projects/16).
- [38] <https://www.digitalrockportal.org/projects/16>.

- [39] J. Gostick, Z. Khan, T. Tranter, M. Kok, M. Agnaou, M. Sadeghi, and R. Jervis, Porespy: A python toolkit for quantitative analysis of porous media images, [J. Open Source Softw.](#) **4**, 1296 (2019).
- [40] V. Robins, M. Saadatfar, O. Delgado-Friedrichs, and A. P. Sheppard, Percolating length scales from topological persistence analysis of micro-CT images of porous materials, [Water Resour. Res.](#) **52**, 315 (2016).
- [41] R. M. Sok, M. A. Knackstedt, A. P. Sheppard, W. V. Pinczewski, W. Lindquist, A. Venkatarangan, and L. Paterson, Direct and stochastic generation of network models from tomographic images; effect of topology on residual saturations, [Transp. Porous Media](#) **46**, 345 (2002).
- [42] J.-Y. Arns, V. Robins, A. P. Sheppard, R. M. Sok, W. V. Pinczewski, and M. A. Knackstedt, Effect of network topology on relative permeability, [Transp. Porous Media](#) **55**, 21 (2004).
- [43] V. Robins, P. J. Wood, and A. P. Sheppard, Theory and algorithms for constructing discrete Morse complexes from grayscale digital images, [IEEE Trans. Pattern Anal.](#) **33**, 1646 (2011).
- [44] A. Suzuki, M. Miyazawa, A. Okamoto, H. Shimizu, I. Obayashi, Y. Hiraoka, T. Tsuji, P. Kang, and T. Ito, Inferring fracture forming processes by characterizing fracture network patterns with persistent homology, [Comput. Geosci.](#) **143**, 104550 (2020).